Organic LETTERS

Letter

pubs.acs.org/OrgLett

Characterization of a Brain Permeant Fluorescent Molecule and Visualization of Aβ Parenchymal Plaques, Using Real-Time Multiphoton Imaging in Transgenic Mice

G.S.M. Sundaram,[†,‡] Kanchan Garai,[§] Nigam P. Rath,[○] Ping Yan,[∥] John R. Cirrito,[∥,#,▽] Nigel J. Cairns,[∥,⊥,#] Jin-Moo Lee,[‡,§,∥] and Vijay Sharma*[,†,‡,§]

[†]BRIGHT Institute, Molecular Imaging Center, [‡]Mallinckrodt Institute of Radiology, [§]Department of Biomedical Engineering, [∥]Departments of Neurology and [⊥]Pathology & Immunology, [#]Knight Alzheimer's Disease Research Center, and [▽]Hope Center for Neurological Disorders, Washington University School of Medicine, St. Louis, Missouri 63110, United States

[○]Departments of Chemistry & Biochemistry, University of Missouri, St. Louis, Missouri 63121, United States

Supporting Information

ABSTRACT: Emerging paradigms mandate discovery of imaging agents for diagnosing Alzheimer's disease (AD) prior to appearance of clinical symptoms. To accomplish this objective, a novel heterocyclic molecule (**4**) was synthesized and validated as Aβ targeted probe. The agent shows labeling of numerous diffuse Aβ plaques in confirmed AD human brain tissues and traverses the blood−brain barrier to enable labeling of parenchymal Aβ plaques in live mice (APP[±]/PS1[±]) brains.

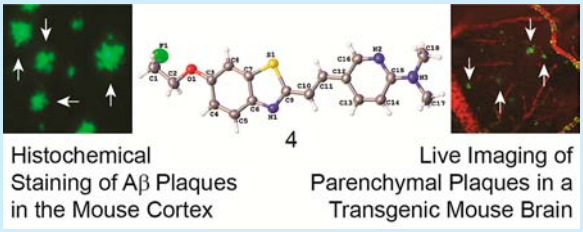

Alzheimer's disease (AD) is the most frequent form of dementia, which affects 24 million people worldwide and also lacks effective therapeutic interventions.[1] The failure of clinical drug trials to reverse clinical symptoms indicates that for a given treatment to be effective, it most likely needs to be prescribed at a preclinical stage before the symptomatic expression of the disease. Therefore, there is an urgent need to identify and validate biomarkers present at preclinical stages of this disease. AD is characterized neuropathologically by β-amyloid (Aβ) plaques and intraneuronal accumulations of abnormal neurofibrillary tangles (NFTs), composed of the tau protein.[2] In vitro and rodent models indicate that the accumulation of $A\beta_{1-42}$ and $A\beta_{1-40}$ fragments may lead to neuronal and synaptic loss, resulting in cognitive decline. Additionally, model systems indicate that Aβ aggregation is an initiating event in the AD pathogenic cascade: (a) overexpression of amyloid precursor protein (APP; a transmembrane protein encoded on chromosome 21) is a characteristic of Down Syndrome (DS);[3] (b) missense mutations in APP also induce an elevation of Aβ levels;[4,5] (c) mutations in the presenilin (*PSEN1* and *PSEN2*) genes have been shown to increase the expression of variant $A\beta_{1-42}$;[5,6] and (d) transgenic mice overexpressing APP develop AD-like neuropathology.[7] Overall, there is ample evidence that suggests AD pathological changes (Aβ deposition and NFT formation) occur years prior to onset of symptoms.[8] While all these observations suggest that Aβ plaque formation occurs decades prior to the beginning of neurodegeneration phase, the temporal relationship between amyloid deposition, neuronal loss, and cognitive decline are intensely debated and continuously investigated. Therefore, for elucidation of these relationships, early diagnosis of AD and the efficient assessment of disease modifying treatments, a noninvasive PET imaging technique to quantify brain amyloid deposition is desired.

Toward this objective, radiopharmaceuticals such as, [^{11}C]2-(4′-methylaminophenyl)-6-hydroxybenzothiazole, ([^{11}C]PIB),[9] 2-(1-(6-((2[^{18}F]fluoroethyl)methylamino)-2-naphthyl)-ethylidene)malononitrile ([^{18}F]FDDNP),[10] [^{11}C]4-*N*-methylamino-4′-hydroxystilbene (SB-13),[11] and (*E*)-4-(2-(6-(2-(2-[^{18}F]-fluoroethoxy)ethoxy)ethoxy)pyridin-3-yl)vinyl)-*N*-methylbenzenamine ([^{18}F]Avid45),[12] and 2-(2-fluoro-6-(methylamino)pyridine-3-yl)benzofuran-6-ol([^{18}F]-AZD4694)[13,14] have been investigated in humans using PET imaging. In addition, [^{125}I/^{131}I]TZDM and [^{125}I]IMPY have also been investigated for SPECT applications.[10] While [^{11}C]PIB has been most intensely studied, [^{18}F]Avid45 and ^{18}F-flutemetamol[15,16] were recently approved by FDA for Aβ imaging. Importantly, both [^{18}F]Avid45[17] and [^{11}C]PIB show promising results in humans and excellent correlation with FDG.[9] While showing merit, each of these agents has demonstrated shortcomings worthy of consideration. Among these limitations, [^{11}C]PIB,[18] [^{11}C]SB-13,[11] and [^{18}F]Avid45[12] have demonstrated low biological half-lives in serum. While metabolites of PIB have been postulated to not penetrate the brain,[18] two metabolites of [^{18}F]Avid45 (desmethylated, 4.5%ID/g; acetylated analogue, 3.3%ID/g at 2 min in normal mice)[12] have been shown to permeate the brain, which could complicate the analysis. Additionally, systematic investigations of [^{3}H]PIB (at tracer concentrations comparable with PET imaging) binding to human neuropathological brain specimens indicate the inter-

Received: May 5, 2014
Published: July 8, 2014

dx.doi.org/10.1021/ol501264q | *Org. Lett.* 2014, 16, 3640−3643

action of a radiotracer with classical Aβ plaques, NFTs (intensity is low compared with Aβ pathology), and cerebrovascular amyloid angiopathy (CAA).[19] The other Aβ imaging agent, [^{18}F]FDDNP, shows binding to NFTs, prion plaques, and fibrillar Aβ, therefore indicating a lack of specificity toward probing AD.[10,20] Significantly, all agents demonstrate considerable white matter binding ([^{18}F]Avid45 shows 2-fold higher binding than [^{11}C]PIB), thus providing challenges for analysis in early stages of AD. Noticeably, [^{11}C]PIB has been unable to detect cerebral Aβ in some patients.[21] Overall, existing agents have not demonstrated sensitivity to detect the earliest Aβ pathophysiology to enable benefits at preclinical stages. Therefore, F-18-incorporated ultrasensitive PET probes capable of targeting highly prevalent sites on Aβ yet displaying faster kinetics from nontargeted regions (high signal-to-noise ratio), minimal white matter interaction, and targeting diffuse- as well as Aβ fibrillar plaques could provide a quantitative amyloid imaging test for guiding management of AD. Herein, we report chemical characterization and crystal structure of the molecule **4** ((*E*)-5-(2-(6-(2-fluoroethoxy)benzo[*d*]thiazol-2-yl)vinyl)-*N*,*N*-dimethylpyridin-2-amine), its preliminary assessment of target specificity in mice and human tissues. Within minutes post-intravenous injection, **4** penetrates the BBB to label Aβ plaques in brains of APP$^{\pm}$/PS1$^{\pm}$ mice.

Our strategic design for generation of an Aβ-targeted agent involved five functional components: (a) a benzothiazole moiety without the methyl group on the heterocyclic nitrogen of thioflavin T to remove the positive charge for enhancing affinity of the probe to Aβ plaques and hydrophobicity to facilitate BBB penetration; (b) modifications of substituents on the sixth position of the benzothiazole ring insignificantly impact affinity of probes for plaques; (c) introduction of an olefin bond between the benzothiazole moiety and an aromatic ring to increase electron density as well as flexibility of the molecule to promote interactions with binding sites present on both diffuse and fibrillar Aβ plaques; (d) substituting a basic dimethylamino group into an aromatic ring at the *para* position to the olefinic carbon to increase electron density on the nitrogen; and (e) incorporation of a heteroatom, such as nitrogen atom in the aromatic ring ortho to the basic dimethylamino group, to enable better resonance stabilization for influencing $\pi-\pi$ interactions for targeting of high density and moderate affinity sites on Aβ plaques. When the above-mentioned characteristic features were incorporated into a template scaffold, compound **4** was synthesized as shown in Scheme 1 (synthetic chemistry details in Supporting Information).

For synthesis, 6-methoxy-2-methylbenzothiazole (**1**) was obtained using literature procedures[22] and condensed with 6-(dimethylamino)nicotinaldehyde in an aqueous potassium hydroxide (50%) solution dissolved in DMSO to obtain **2**. Following purification, **2** was demethylated in the presence of BBr_3 to yield the phenolic derivative **3**. Finally, **3** was alkylated with 2-fluoroethyl-4-methylbenzenesulfonate (prepared using

Scheme 1. Chemical Synthesis of Heterocyclic Molecule 4

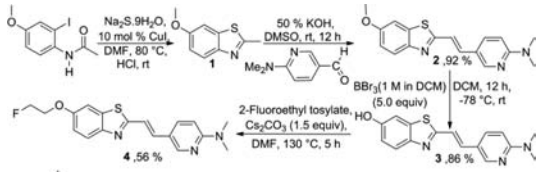

Figure 1. Projection view of **4** showing the crystallographic numbering scheme of atoms (thermal ellipsoids: 50% probability).

literature procedure[23]) in the presence of cesium carbonate to obtain **4**. All intermediates, **1**, **2**, **3**, and the final compound **4**, were characterized via standard analytical methods. Additionally, **4** was also analyzed for uniformity and purity, on a semi-preparative C-18 column (Vydac), using an HPLC system. Compound **4** eluted as a single chemical entity, with a retention time of 10 min, thus indicating purity of the molecule. The organic molecule **4** crystallized in a triclinic space group *P*1. The ORTEP drawing showing the crystallographic numbering scheme for **4** is illustrated in Figure 1. The crystal structure indicates a nearly planar molecule with a calculated root-mean-square deviation of 0.062 Å for the entire core (all atoms except the H and F atoms) and also indicates a weak $\pi-\pi$ interaction and hydrogen bonding (Supporting Information, Figure 2). The NMR spectral data of **4** were also consistent with the crystal structure, thus indicating the presence of identical structures both in solid and solution state.

For assessing the ability of **4** to bind Aβ plaques, preliminary binding assays with preformed Aβ_{1-42} aggregates were performed. Following excitation at 410 nm, the fluorescence spectrum of **4** recorded in PBS showed an emission peak with E_{max} at 503 nm. Upon incubation with preformed aggregates of Aβ_{1-42}, the peak at 503 nm shifted slightly (E_{max} 485 nm) and simultaneously demonstrated a remarkable enhancement in the fluorescence, due to binding to Aβ aggregates (Supporting Information, Figure 3). This enhancement in fluorescence upon interaction with Aβ_{1-42} fibrils is consistent with profiles observed with other fluorescent molecules under similar conditions.[24] Additionally, no fluorescence was observed using Aβ aggregates alone in PBS following excitation at 410 nm (negative control). Overall, binding assay of **4** with preformed Aβ_{1-42} aggregates indicates a nearly saturable binding with K_d = 59 ± 7 nM (Supporting Information, Figure 4).

The double-transgenic mice having coexpression of the mutated genes (APP$^{\pm}$/PS1$^{\pm}$) exhibit a strikingly accelerated accumulation of Aβ deposits compared with the single APP transgenic counterparts.[25−,27] Noticeably, several Aβ ligands and disease-modifying therapeutics have been investigated for their efficacy using APP$^{\pm}$/PS1$^{\pm}$ mice.[28,29] Further, we assessed the ability of **4** to stain ex vivo brain sections (50 μm) of age-matched APP$^{\pm}$/PS1$^{\pm}$ mice and their WT (BL/6) counterparts, using established procedures.[30] As a positive control, anti-Aβ monoclonal antibody (mHJ3.4 conjugated to Alexa 568) was used.[31] Brain sections of 24-month-old APP$^{\pm}$/PS1$^{\pm}$ mice showed abundant staining of Aβ (Figure 2) compared with none in WT counterparts (data not shown). Similarly, **4** (1 μM) demonstrated abundant staining of fibrillar plaques in the cortical regions of brain sections (Figure 2) in APP$^{\pm}$/PS1$^{\pm}$ mice. By comparison, **4** showed no staining in WT mice (Supporting Information, Figure 5), thus indicating its target specificity. Finally, **4** also showed significant correlation (Figure 2; merged image) with anti-Aβ antibody. However, a slightly less than 1:1 correlation in the merged image could be attributed to binding patterns of **4**, a small organic molecule versus an anti-Aβ antibody.

dx.doi.org/10.1021/ol501264q | *Org. Lett.* 2014, 16, 3640−3643

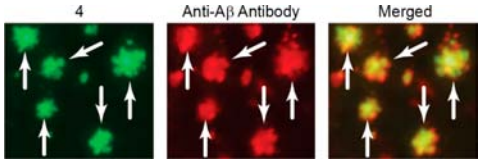

Figure 2. Staining of brain tissue sections (50 μm) from APP$^{\pm}$/PS1$^{\pm}$ mice using **4** (1 μM) or immunostained with mouse anti-Aβ monoclonal antibody (mHJ3.4) conjugated to Alexa Fluor 568 (positive control). Arrows indicate labeling of Aβ plaques. Similar results were obtained in more than five independent experiments.

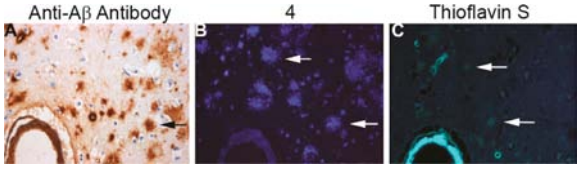

Figure 3. Binding of anti-Aβ antibody (10D5, Eli Lilly, A), **4** (B), and thioflavin S (C) to Aβ plaques in AD brain near/adjacent tissue sections. Amyloid in post-mortem frontal lobe of a 90-year-old male. Magnification: 200×. (A) Diffuse Aβ plaques and an arteriole with Aβ deposits (cerebral amyloid angiopathy); 10D5 immunohistochemistry. (B) Section stained with **4** containing the same arteriole as in (A). There are numerous diffuse Aβ plaques and the vessel is also stained. (C) Thioflavin S reveals amyloid in blood vessels but diffuse plaques are only weakly stained. The same diffuse Aβ plaque is labeled in A–C. Similar results were obtained in more than five independent cases.

Despite showing promising affinity in vitro, initial good penetration as well as clearance in normal mice, and staining to transgenic mice brain cross-sections, few Aβ-targeted ^{99m}Tc-ligands have not displayed any binding with Aβ plaques in human tissues, thus impeding their further development.[32] To further assess the ability of **4** to label Aβ plaques in human brain, staining experiments were performed with post-mortem tissues from clinically characterized AD patients.[33,34] As a positive control, a highly specific anti-Aβ antibody (10 D5, Eli Lilly, Indianapolis, IN) was used to ascertain the presence of Aβ plaques (Figure 3A), using well-established procedures.[35] Importantly, **4** (10 μM) demonstrated strikingly distinct labeling of Aβ plaques in the tissue sections of frontal lobe of a 90-year-old male with AD (Figure 3) and absence of Aβ plaques in normal controls (Supporting Information, Figure 6), thus indicating target specificity. Noticeably, **4** also indicated proficient and distinct labeling of plaque and leptomeningeal vessels (cerebral amyloid angiopathy; CAA) (Figure 3B). These data are consistent with other unlabeled counterparts of FDA-approved PET agents.[36] Furthermore, thioflavin S, an amyloid staining dye, showed staining of amyloid in the blood vessel (CAA) and indicated only weak staining of diffuse plaques (Figure 3C). Importantly, **4** demonstrated labeling of numerous diffuse Aβ plaques (Figure 3B). Overall, the ability and sensitivity of **4** to detect diffuse plaques could represent an important advancement to enable PET imaging of mildly demented individuals prior to onset of symptoms.[8]

The discovery and development of new ligands to enable imaging of biomarkers in brain mandates interrogation of their ability to permeate the BBB, excretion from nearby nontargeted regions of the brain to provide a high signal/noise ratio, and specificity for a given target. For assessing viability of molecules as imaging probes in vivo,[37] various imaging modalities, such as nuclear imaging (PET/SPECT), optical imaging, and MRI have been used to investigate simultaneously distribution kinetics and target-receptor specificity. While the resolution of PET and MRI allow in vivo imaging at relatively lower resolution, the multiphoton microscopy enables precise evaluation of the specificity of a given ligand binding to its target at a submicrometer resolution.[38] Therefore, this technique enables characterization of probes in small animal models at a significantly high spatial and temporal resolution.[38]

For assessing the ability of **4** to penetrate the BBB, label Aβ parenchymal plaques, and simultaneously interrogate the pharmacokinetic profiles from nearby brain regions, direct real-time imaging was performed in transgenic APP$^{\pm}$/PS1$^{\pm}$ mice. Prior to imaging, dextran–Texas Red conjugate (33 mg/kg; dissolved in PBS to mark the blood vessels) and **4** (2 mg/kg; dissolved in 20% DMSO in propylene glycol[39]) were intravenously administered to anesthetized APP$^{\pm}$/PS1$^{\pm}$ mice (with cranial windows; Supporting Information). Compared with barely detectable autofluorescence levels in either vehicle treated BL6 (WT) mice (data not shown) or prior to imaging transgenic APP$^{\pm}$/PS1$^{\pm}$ mice (Figure 4), bright fluorescence appeared in large and small blood vessels of the brain following injection. Within minutes, the fluorescent molecule crossed the BBB and entered the brain parenchyma and Aβ deposits were labeled. While the complete labeling of CAA occurred instantaneously following injection, the labeling of parenchymal plaques peaked at approximately 10 min. Overall, these data demonstrate in real time that **4** enters the CNS rapidly and labels parenchymal Aβ plaques. These real-time pharmacokinetic data in transgenic mice provide an ideal platform for PET tracer development.

In summary, novel heterocyclic fluorescent molecule **4** demonstrates binding to both diffuse and fibrillar Aβ plaques, a promising feature that could enable diagnosis of AD at preclinical stages. Multiphoton imaging shows real-time pharmacokinetics of **4** in brains of transgenic mice at a highest resolution, penetration of the BBB, and ability of the agent to label Aβ plaques in brain parenchyma and blood vessels (CAA). Additionally, the low level of background fluorescence from residual retention of **4** suggests high signal-to-background ratios, an asset for PET imaging applications. Although imaging of **4** with multiphoton microscopy does not predict the sensitivity levels obtainable with tracer imaging, the technique allows detection of individual plaques within a very small volume of the brain compared with PET imaging probes that provide an averaged intensity of Aβ binding at a low spatial resolution. Thus,

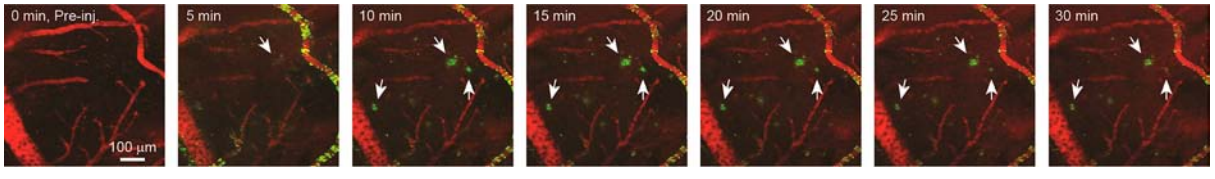

Figure 4. Real time imaging of **4** in brains of APP $^{\pm}$/PS1$^{\pm}$ transgenic mice: Following labeling of blood vessels with dextran-Texas Red, **4** (2 mg/kg) was intravenously injected. A z-stack image series was acquired using an LSM 510META NLO microscope (Carl-Zeiss Inc.).

dx.doi.org/10.1021/ol501264q | Org. Lett. 2014, 16, 3640–3643

the sensitivity of **4** for detection of Aβ with PET imaging will need to be addressed independently. Nevertheless, these data provide a provocative platform technology for development of PET tracers to enable noninvasive assessment of Aβ plaques in vivo. Further investigations on a PET counterpart of **4** are under investigation.

■ ASSOCIATED CONTENT

Supporting Information

Experimental and synthetic procedures (**1**−**4**), analytical data, and X-ray crystallographic data for **4**. This material is available free of charge via the Internet at http://pubs.acs.org.

■ AUTHOR INFORMATION

Corresponding Author

*Tel: 314-362-9358. E-mail: sharmav@mir.wustl.edu.

Notes

The authors declare no competing financial interest.

■ ACKNOWLEDGMENTS

Financial assistance for this work was provided by grants from the National Institutes of Health in part by AG030498 (V.S.) and AG033328 (V.S.), P50-AG05681, P01-AG03991 (N.J.C.), and MIR funds (V.S.).

■ REFERENCES

(1) Ferri, C. P.; Prince, M.; Brayne, C.; Brodaty, H.; Fratiglioni, L.; Ganguli, M.; Hall, K.; Hasegawa, K.; Hendrie, H.; Huang, Y.; Jorm, A.; Mathers, C.; Menezes, P. R.; Rimmer, E.; Scazufca, M. *Lancet* **2005**, *366*, 2112−7.

(2) Roher, A. E.; Cribbs, D. H.; Kim, R. C.; Maarouf, C. L.; Whiteside, C. M.; Kokjohn, T. A.; Daugs, I. D.; Head, E.; Liebsack, C.; Serrano, G.; Belden, C.; Sabbagh, M. N.; Beach, T. G. *PloS One* **2013**, *8*, e59735.

(3) Teller, J.; Russo, C.; Debusk, L.; Angelini, G.; Zaccheo, D.; Dagna-Bricarelli, F.; Scartezzini, P.; Bertolini, S.; Mann, D.; Tabaton, M.; Plerluigi, G. *Nat. Med.* **1996**, *2*, 93−95.

(4) Selkoe, D. *J. Biol. Chem.* **1996**, *271*, 18295−18298.

(5) Selkoe, D. *Science* **1997**, *275*, 630−631.

(6) Lemere, C.; Lopera, F.; Kosik, K.; Lendon, C.; Ossa, J.; Saido, T.; Yamaguchi, H.; Ruiz, A.; Martinez, A.; Madrigal, L.; Hincapie, L.; Anthony, D.; Koo, E.; Goate, A.; Selkoe, D.; Arango, C. *Nat. Med.* **1996**, *2*, 1146−1150.

(7) Hsiao, K.; Chapman, P.; Nilsen, S.; Eckman, S.; Harigaya, Y.; Younkin, S.; Yang, F.; Cole, G. *Science* **1996**, *274*, 99−102.

(8) Price, J. L.; McKeel, D. W., Jr.; Buckles, V. D.; Roe, C. M.; Xiong, C.; Grundman, M.; Hansen, L. A.; Petersen, R. C.; Parisi, J. E.; Dickson, D. W.; Smith, C. D.; Davis, D. G.; Schmitt, F. A.; Markesbery, W. R.; Kaye, J.; Kurlan, R.; Hulette, C.; Kurland, B. F.; Higdon, R.; Kukull, W.; Morris, J. C. *Neurobiol. Aging* **2009**, *30*, 1026−36.

(9) Klunk, W.; Engler, H.; Nordberg, A.; Wang, Y.; Blomqvist, G.; Holt, D.; Bergstrom, M.; Savitvheva, I.; Huang, G.; Estrada, S.; Ausen, B.; Bebnath, M.; Barletta, J.; Price, J.; Sandell, J.; Lopresti, B.; Wall, A.; Koivisto, P.; Antoni, G.; Mathis, C.; Langstrom, B. *Ann. Neurol.* **2004**, *55*, 306−319.

(10) Nordberg, A. *Lancet Neurol.* **2004**, *3*, 519−527.

(11) Verhoeff, N.; Wilson, A.; Takeshita, S.; Trop, L.; Hussey, D.; Singh, K.; Kung, H.; Kung, M.; Houle, S. *Am. J. Geriatr. Psychiatry* **2004**, *12*, 584−595.

(12) Choi, S. R.; Golding, G.; Zhuang, Z.; Zhang, W.; Lim, N.; Hefti, F.; Benedum, T. E.; Kilbourn, M. R.; Skovronsky, D.; Kung, H. F. *J. Nucl. Med.* **2009**, *50*, 1887−94.

(13) Rowe, C. C.; Pejoska, S.; Mulligan, R. S.; Jones, G.; Chan, J. G.; Svensson, S.; Cselenyi, Z.; Masters, C. L.; Villemagne, V. L. *J. Nucl. Med.* **2013**, *54*, 880−6.

(14) Cselenyi, Z.; Jonhagen, M. E.; Forsberg, A.; Halldin, C.; Julin, P.; Schou, M.; Johnstrom, P.; Varnas, K.; Svensson, S.; Farde, L. *J. Nucl. Med.* **2012**, *53*, 415−24.

(15) Koole, M.; Lewis, D. M.; Buckley, C.; Nelissen, N.; Vandenbulcke, M.; Brooks, D. J.; Vandenberghe, R.; Van Laere, K. *J. Nucl. Med.* **2009**, *50*, 818−22.

(16) Nelissen, N.; Van Laere, K.; Thurfjell, L.; Owenius, R.; Vandenbulcke, M.; Koole, M.; Bormans, G.; Brooks, D. J.; Vandenberghe, R. *J. Nucl. Med.* **2009**, *50*, 1251−9.

(17) Wong, D. F.; Rosenberg, P. B.; Zhou, Y.; Kumar, A.; Raymont, V.; Ravert, H. T.; Dannals, R. F.; Nandi, A.; Brasic, J. R.; Ye, W.; Hilton, J.; Lyketsos, C.; Kung, H. F.; Joshi, A. D.; Skovronsky, D. M.; Pontecorvo, M. J. *J. Nucl. Med.* **2010**, *51*, 913−20.

(18) Mathis, C.; Wang, Y.; Holt, D.; Huang, G.; Debnath, M.; Klunk, W. *J. Med. Chem.* **2003**, *46*, 2740−2754.

(19) Lockhart, A.; Lamb, J. R.; Osredkar, T.; Sue, L. I.; Joyce, J. N.; Ye, L.; Libri, V.; Leppert, D.; Beach, T. G. *Brain* **2007**, *130*, 2607−15.

(20) Agdeppa, E.; Kepe, V.; Petric, A.; Satyamurthy, N.; Liu, J.; Huang, S.; Small, G.; Cole, G.; Barrio, J. *Neuroscience* **2003**, *117*, 723−730.

(21) Cairns, N. J.; Ikonomovic, M. D.; Benzinger, T.; Storandt, M.; Fagan, A. M.; Shah, A. R.; Reinwald, L. T.; Carter, D.; Felton, A.; Holtzman, D. M.; Mintun, M. A.; Klunk, W. E.; Morris, J. C. *Arch. Neurol.* **2009**, *66*, 1557−62.

(22) Ma, D.; Xie, S.; Xue, P.; Zhang, X.; Dong, J.; Jiang, Y. *Angew. Chem., Int. Ed.* **2009**, *48*, 4222−5.

(23) Yu, K.; Park, J.; Yang, S. *Bull. Korean Chem. Soc.* **2004**, *25*, 506−510.

(24) Klunk, W.; Wang, Y.; Hunag, G.; Debnath, M.; Holt, D.; Mathis, C. *Life Sci.* **2001**, *69*, 1471−1484.

(25) McGowan, E.; Sanders, S.; Iwatsubo, T.; Takeuchi, A.; Saido, T.; Zehr, C.; Yu, X.; Uljon, S.; Wang, R.; Mann, D.; Dickson, D.; Duff, K. *Neurobiol. Dis.* **1999**, *6*, 231−44.

(26) Holcomb, L.; Gordon, M. N.; McGowan, E.; Yu, X.; Benkovic, S.; Jantzen, P.; Wright, K.; Saad, I.; Mueller, R.; Morgan, D.; Sanders, S.; Zehr, C.; O'Campo, K.; Hardy, J.; Prada, C. M.; Eckman, C.; Younkin, S.; Hsiao, K.; Duff, K. *Nat. Med.* **1998**, *4*, 97−100.

(27) Trinchese, F.; Liu, S.; Battaglia, F.; Walter, S.; Mathews, P. M.; Arancio, O. *Ann. Neurol.* **2004**, *55*, 801−14.

(28) Carrera, I.; Etcheverria, I.; Fernandez-Novoa, L.; Lombardi, V.; Cacabelos, R.; Vigo, C. *Int. J. Alzheimer's Dis* **2012**, *2012*, 376138.

(29) Tanifum, E. A.; Dasgupta, I.; Srivastava, M.; Bhavane, R. C.; Sun, L.; Berridge, J.; Pourgarzham, H.; Kamath, R.; Espinosa, G.; Cook, S. C.; Eriksen, J. L.; Annapragada, A. *PloS One* **2012**, *7*, e48515.

(30) DeMattos, R. B.; O'dell, M. A.; Parsadanian, M.; Taylor, J. W.; Harnony, J. A.; Bales, K. R.; Paul, S. M.; Aronow, B. J.; Holtzman, D. *Proc. Natl. Acad. Sci. U.S.A.* **2002**, *99*, 10843−10848.

(31) Cirrito, J. R.; Disabato, B. M.; Restivo, J. L.; Verges, D. K.; Goebel, W. D.; Sathyan, A.; Hayreh, D.; D'Angelo, G.; Benzinger, T.; Yoon, H.; Kim, J.; Morris, J. C.; Mintun, M. A.; Sheline, Y. I. *Proc. Natl. Acad. Sci. U.S.A.* **2011**, *108*, 14968−73.

(32) Zhuang, Z.; Kung, M.; Hou, C.; Ploessl, K.; Kung, H. *Nucl. Med. Biol.* **2005**, *32*, 171−184.

(33) Mirra, S.; Heyman, A.; McKeel, D.; Sumi, S.; Crain, B.; Brownlee, L.; Vogel, F.; Hughes, J.; van Belle, G.; Berg, L. *Neurology* **1991**, *41*, 479−486.

(34) Hyman, B.; Trojanowski, J. *J. Neuropathol. Exp. Neurol.* **1997**, *56*, 1095−1097.

(35) Cairns, N. J.; Taylor-Reinwald, L.; Morris, J. C. *Alzheimer's Dement.* **2010**, *6*, 274−9.

(36) Mathis, C. A.; Mason, N. S.; Lopresti, B. J.; Klunk, W. E. *Semin. Nucl. Med.* **2012**, *42*, 423−32.

(37) Quillard, T.; Libby, P. *Circ. Res.* **2012**, *111*, 231−44.

(38) Dong, J.; Revilla-Sanchez, R.; Moss, S.; Haydon, P. G. *Neuropharmacology* **2010**, *59*, 268−75.

(39) Bacskai, B.; Hickey, G.; Skoch, J.; Kajdasz, S.; Wang, Y.; Huang, G.; Mathis, C.; Klunk, W.; Bradley, T. *Proc. Natl. Acad. Sci. U.S.A.* **2003**, *100*, 12462−12467.